IEEE Access
Multidisciplinary | Rapid Review | Open Access Journal

SPECIAL SECTION ON DATA-ENABLED INTELLIGENCE FOR DIGITAL HEALTH

Received November 19, 2019, accepted December 8, 2019, date of publication December 19, 2019,
date of current version December 31, 2019.

Digital Object Identifier 10.1109/ACCESS.2019.2960844

End-to-End Blood Pressure Prediction via Fully Convolutional Networks

SANGHYUN BAEK[1,2], JIYONG JANG[1,3], AND SUNGROH YOON[1,4], (Senior Member, IEEE)

[1]Department of Electrical and Computer Engineering, Seoul National University, Seoul 08826, South Korea
[2]Mobile Business, Samsung Electronics Company Ltd., Suwon 16677, South Korea
[3]Global Technology Center, Samsung Electronics Company Ltd., Suwon 16677, South Korea
[4]ASRI, INMC, ISRC, and Institute of Engineering Research, Seoul National University, Seoul 08826, South Korea

Corresponding author: Sungroh Yoon (sryoon@snu.ac.kr)

This work was supported in part by the National Research Foundation of Korea (NRF) through the Korea Government (Ministry of Science and ICT) under Grant 2018R1A2B3001628, in part by the Brain Korea 21 Plus Project in 2019, and in part by Samsung Electronics Company, Ltd.

ABSTRACT Cardiovascular disease is the leading cause of death in the world. It is vital to prevent it by rapid diagnosis and appropriate management through periodic blood pressure (BP) measurement. Recently, many studies have been conducted on methods to measure BP without a cuff. One of the most common methods of predicting BP without a cuff is to use the correlation between pulse wave velocity (PWV) and BP. Studies that predict BP through PWV have two problems to overcome: 1) Additional efforts are required to extract PWV features manually from various biomedical signals, such as electrocardiogram (ECG) and photoplethysmogram (PPG); and 2) in predicting BP using biomedical signals from other people, individual periodic calibration is required because the correlation between PWV and BP differs from person to person. In this study, we proposed a cuffless BP prediction method based on a deep convolutional neural network (CNN) that can overcome the problems mentioned above. The proposed CNN method 1) can use raw signals for training without PWV feature extraction; and 2) automatically learns the characteristics of biomedical signals from other people to predict BP accurately without calibration. We propose two schemes: extraction through multiple dilated convolution, and concentration through strided convolution with a large kernel, to process sequential ECG and PPG signals through CNN. BP prediction performance was the best when both ECG and PPG signals were used together. To this end, we conducted extensive experiments on the different settings of the proposed method and constructed an effective learning model. The proposed method achieved excellent performance in predicting both systolic blood pressure and diastolic blood pressure over other known approaches. We also verified that the performance of our method fulfills international standard protocols, AAMI, and BHS.

INDEX TERMS Biomedical signal processing, computational and artificial intelligence, health information management, machine learning, cuffless blood pressure measurement, deep learning, convolutional neural networks, end-to-end.

I. INTRODUCTION

High blood pressure (BP) is a common and dangerous condition. About 1 out of 3 adults in the U.S. (about 75 million people) have high BP. This common condition increases the risk of heart disease and stroke, two of the leading causes of death for Americans [1], [2]. High BP is called the ''silent killer'' because it often has no warning signs or symptoms, and many people are not aware they have it. For this reason it is important to check BP regularly.

The associate editor coordinating the review of this manuscript and approving it for publication was Linbo Qing.

Traditional BP measurement is based on the cuff. When using this method, BP cannot be re-measured until the occluded artery returns to its original position. It is not suitable for continuous BP measurement or observation of long-term BP change. The pressure of the cuff may also cause the subject to feel uncomfortable or to suffer skin trauma. To overcome these shortcomings, improvements in cuffless and continuous BP estimation methods have been an area of recent research.

Cuffless BP measurement is an all-inclusive term for a method that aims to measure BP without using a cuff. The most common method for cuffless BP measurement is based

on manual examination of pulse wave velocity (PWV) features [3], [4]. PWV is the velocity of the pressure wave flowing through the blood vessels. This PWV based method can predict the blood pressure value by using the relationship between the time required for the blood to move between two points and the distance between these points. To measure the time value in a noninvasive manner, various biomedical signals, such as electrocardiogram (ECG), photoplethysmogram (PPG), ballistocardiogram (BCG) and seismocardiogram (SCG) are used [5]. A number of studies have shown that ECG and PPG signals are the most commonly used to effectively predict BP. The time values are referred to as pulse arrival time (PAT) or pulse transit time (PTT). PAT refers to the time difference between the R-peak of the ECG signal and the PPG peak, and is usually obtained from the ECG signal and the PPG signal measured at one of the wrists, ankles, or other in vitro sites. PTT refers to the time it takes for a blood pressure-induced waveform to travel between two points in the artery, usually measured through PPG sensor signals. However, as described earlier in this paper, the PWV-based method requires recognizing features from the signal waveforms, and thus additional effort. This method also requires either a combination of simultaneously measured ECG and PPG or two simultaneously measured PPGs, which is inconvenient and cumbersome. Furthermore, the PWV-based method usually requires an elaborate individual calibration process using a sphygmomanometer with a cuff because the correlation between PWV features and BP varies from person to person [6], [7], [8], and thus cannot be used as a replacement for a cuff sphygmomanometer. There are some limitations with collecting ECG and PPG simultaneously using a mobile device.

As another way to predict BP without a cuff, some researchers have attempted to predict BP using a single raw biomedical signal or transform rather than the PWV-based feature [9], [10], [11], [12]. The concept of predicting BP using a single signal measurement such as ECG or PPG appears to be more appropriate for mobile devices such as smartphones and smart watches. A non-PWV based method can be relatively accurate without calibration because the method finds the characteristics which can predict BP in the biomedical signal itself without using the correlation between PWV and BP which is different from person to person. However, it is difficult to obtain high BP prediction accuracy using this method.

In this paper, we devised a method of BP prediction based on a deep convolutional neural network (CNN). The proposed method can overcome the drawbacks of feature recognition of the PWV-based method and the low BP prediction accuracy of non-PWV based method. It can take advantage of being a non-PWV based method with relatively high BP prediction accuracy without calibration. Unlike other studies based on manual recognition of PWV features, by utilizing the advantage of deep learning which automatically extracts features, raw ECG and PPG signals are used intact to reflect the inherent characteristics of the signals themselves. It is also possible to predict relatively accurate BP without individual calibration.

The main contributions of our work are summarized as follows:

- We proposed a novel end-to-end method of predicting blood pressure using only raw signals with no hand-made features.
- Based on the architecture of CNN, our method has the flexibility to deal with input variations (PPG/ECG, Time/Frequency) and applicability to real-world situations.
- The proposed method achieved excellent performance in predicting both systolic and diastolic blood pressure using the MIMIC II dataset compared with other known approaches.

II. BACKGROUND AND RELATED WORK

Algorithms and mathematical models have been proposed and developed to optimize the regression process of BP prediction and calibration of the PWV features/BP. Recently, there have been many studies to predict BP without a cuff. These can be classified into two categories, PWV-based methods (with manual PWV features) and the non-PWV based methods.

A. BP PREDICTION WITH PWV BASED METHODS

Studies have been carried out to improve BP prediction performance using the PWV-based features that were essential in traditional methods. BP refers to the pressure on the arterial wall when sending blood from the heart to the entire body. These arteries expand when the heart contracts (systole) and contract when the heart expands (diastole). The degree of expansion and contraction depends on the elastic modulus of the blood vessel. The following equation [13] expresses the relation between the elastic modulus of the blood vessel and the BP.

$$E = E_0 e^{\alpha_P} \tag{1}$$

In equation (1), E_0 and α are subject-specific parameters of central artery, P is BP.

Assuming that the artery is a connected elastic tube through which blood flows, the relationship between the velocity of the blood flowing along the artery and the elastic modulus of the blood artery is calculated using the Moens-Kortweg equation as follows:

$$PWV = \sqrt{\frac{hE}{\rho d}} \tag{2}$$

In equation (2), h and d are the thickness and diameter of the artery, respectively; ρ is the density of the blood.

Combining these two equations, we can obtain Bramwell-Hills and Moens-Kortweg's equation, explaining the relationship between BP and PWV, which is inversely proportional to

the "Time Delay" for an artery with a length of L [14].

$$PWV = \frac{L}{TimeDelay} = \sqrt{\frac{hE_0 e^{\alpha_P}}{\rho d}} \tag{3}$$

These time delay values are known as PAT or PTT, and can be measured in a noninvasive manner with various biomedical signals.

Kachuee [3] and Su [4] conducted a study to predict BP using PWV features as the main feature along with many other features extracted from biomedical signals. Kachuee extracted features from ECG and PPG signals and performed a study to predict BP in ECG and PPG signals using machine learning techniques, such as regularized linear regression (RLR), support vector machines (SVMs), decision tree regression, adaptive boosting (AdaBoost), and random forest regression (RFR). Mean absolute error (MAE) is used as an evaluation metric. The accuracy of BP prediction was found to be SBP 11.17 $\pm$ 10.09 and DBP 5.35 $\pm$ 6.14 for calibration-free, and SBP 8.21 $\pm$ 5.45 and DBP 4.31 $\pm$ 3.52 for calibration-based, respectively. Su extracted features from the ECG and PPG signals and performed a study to predict BP in ECG and PPG signals through recurrent networks (LSTM), which achieved SBP 3.73 and DBP 2.43 based on the root-mean-square error (RMSE).

B. BP PREDICTION WITH NON-PWV BASED METHODS

There are studies on predicting the BP value or the Hypertension stage in the PPG and/or ECG signal using non-PWV based methods. Khalid [9] extracted features from only PPG signals and performed a study to predict BP using machine learning techniques such as multiple linear regression (MLR), SVM, and decision tree regression. The accuracy of BP prediction was found to be SBP 4.82 $\pm$ 4.31 and DBP 3.25 $\pm$ 4.17. Wang [10] segments a single PPG signal from the raw PPG signal, extracts morphological and spectral features from the signal, and performs experiments to predict SBP and DBP through artificial neural networks (ANN), which achieved SBP 4.02 $\pm$ 2.79 and DBP 2.27 $\pm$ 1.82. Ertugrul [11] uses a spectrogram, which is the magnitude squared of the short-time Fourier transform (STFT) of a PPG and/or ECG signal, and then performed a study to predict BP through the extreme learning machine method (ELM). The accuracy of BP prediction was found to be SBP 4.37 and DBP 3.95. Zhang [12] also extracted features from a PPG signal and performed a study to predict BP using the SVM method, which achieved SBP 11.64 $\pm$ 8.20 and DBP 7.62 $\pm$ 6.78. Tanveer [15] proposed a waveform-based hierarchical artificial neural network–long short-term memory (ANN–LSTM) model for BP estimation that automatically learns features from ECG and PPG signals through ANN and then uses them as inputs to LSTM to predict BP. Liang [16] transforms the PPG signal to a scalogram, which is a plotted RGB image as a graph of time and frequency, using a continuous wavelet transform. Hypertension classification was conducted using the pre-trained CNN (GoogLeNet). This study obtained superior hypertension classification performance compared to the studies considering PWV based features.

C. DEEP LEARNING IN BIOMEDICAL ENGINEERING

Deep learning is a specific type of machine learning, which uses artificial neural networks consisting of many hidden layers to progressively extract higher-level features from raw input. Deep learning automatically learns the optimal features of the raw signal itself without extracting features [17]. Deep learning has been widely used in areas such as image classification [18], speech recognition, natural language processing, and audio recognition. Recently it has been used in the field of biomedical engineering in areas such as bioinformatics, medical image analysis, and biomedical signal analysis [19].

Some researchers have used deep learning in medical applications, such as cancer detection and dementia diagnosis. Sirinukunwattana [20] presents novel locality sensitive deep learning approaches to detect and classify nuclei in routine hematoxylin and eosin (H&E) stained histopathology images of colorectal adenocarcinoma (Colon Cancer), based on CNN. Choi [21] proposes a deep learning based low-cost and high-accuracy diagnostic framework of dementia with the response profile.

III. METHOD

We propose fully convolutional networks constructed using only 1D convolution for BP prediction. The proposed end-to-end 1D CNN model can predict SBP and DBP directly from raw signals without any additional manual feature extraction process, particularly PWV features.

A common deep learning approach for handling sequence data is to use recurrent-based neural networks. However, the signals related to BP (e.g., PPG, ECG, ABP) have a certain periodicity and pattern repetition, and so can be assumed to be grid topology data with wide range locality apart from long term time dependency. Therefore, we constructed a 1D convolution based neural networks to extract wide ranged local features from fixed length input signals and to regress the real numbered targets. The *Extraction-Concentration blocks* are key components of the proposed model, obtained by combining multiple dilated convolution and strided convolution using large kernel sizes [22]. It is possible to extract and concentrate features from the periodic signals.

The proposed BP estimation method consists of the following steps. 1) Data preparation: Prepare data pair (x,y) from the given database $\mathcal{D}$ for CNN training; 2) CNN based prediction model: Feature extraction through proposed *Extraction-Concentration blocks* and prediction with joint loss L_{total}.

A. DATA PREPARATION

1) DATA SAMPLING

The database $\mathcal{D}$ contains a set of raw PPG, ECG, and arterial blood pressure (ABP) signals $R_i = (r_i^{\text{PPG}}, r_i^{\text{ECG}}, r_i^{\text{ABP}})$,

where i is the subject index and each R_i has a different length. For preparing the training dataset, we sampled random segments S_i from the raw signals to make all datasets the same length l_{seg}. Note that $l_{\text{seg}} = 1000$ for the experiments. During the sampling process, we applied two constraints to ABP signals (the true value of the estimation) for minimum refinement. According to NIH/WHO BP classification standard [23], we first apply the BP range criteria, $90 \leq \max(s^{\text{ABP}}) < 180$, $60 \leq \min(s^{\text{ABP}}) < 120$. Next, we exclude abnormal ABP signals through peak analysis, with the peak constraints defined as $\text{len}(p) \geq 5, \text{StdVar}(\Delta p_x) < 5, \text{StdVar}(p_y) < 5$, where peak $p = (p^1, .., p^n)$, p_x^i is the time stamp and p_y^i is the ABP value of the ith peak. Fig. 1. shows the sampling constraints and examples of excluded cases.

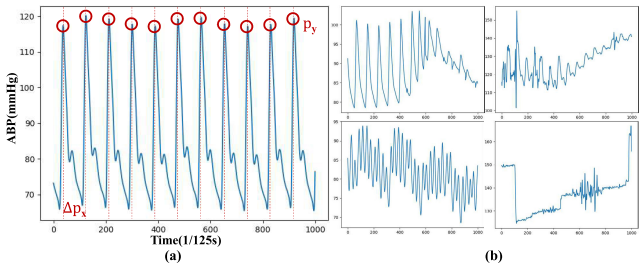

FIGURE 1. Examples of ABP signal for data sampling. (a) Illustration of the sampling constraints. (b) Examples of the false cases.

2) PREPROCESSING

Given segments S from the sampling process, we conducted the preprocessing steps to create adequate input and output data pairs for our method. Three preprocessing techniques are used: random cropping, fast Fourier transform (FFT), and increasing input depth using its derivatives. The preprocessing flow is illustrated in Fig. 2.

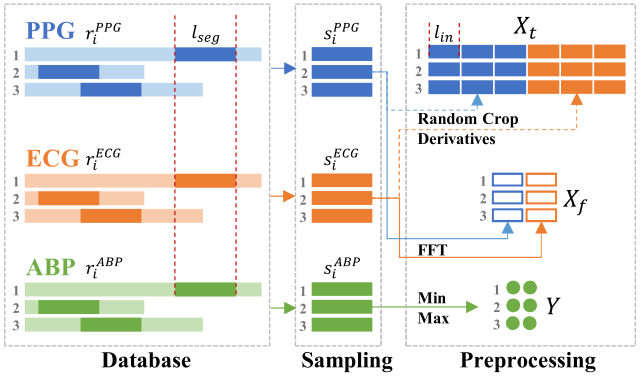

FIGURE 2. Data sampling and preprocessing flow.

To increase the input variation, we use a randomly cropped signal X_t with length l_{in} in the l_{seg}-length segment S. Random cropping allows the model to learn signals at various points in the segment S and to reduce reliance on synchronization between signals. Note that we set $l_{\text{in}} = 512$ in the experiments. Since our model takes both time and frequency domain inputs, the original signal needs to be converted to the frequency domain. FFT is used at this stage; we use Fourier spectrum X_f from the original signal X_t as the input for the frequency encoder. Next, for time domain signals, we increase the input depth by concatenating the input signal's 1st and 2nd derivatives as follows [24].

$$X_t = X_t \oplus \Delta X_t \oplus \Delta^2 X_t \tag{4}$$

The accuracy difference according to the input signal's derivative are shown in Section IV-B.

After the preprocessing step, we end up with a prepared dataset (X_t, X_f, Y) from which we take a mini-batch (x_t, x_f, y) for model training. The dimensions of the prepared dataset in the experiments are $m \times 6 \times 512$, $m \times 2 \times 256$, $m \times 2$ with mini-batch size m for x_t, x_f, y, respectively.

B. CNN BASED PREDICTION MODEL

The overall architecture of the proposed method is shown in Fig. 3. It consists of three parts: a time encoder, a frequency encoder, and three predictors for time, frequency, and combined feature matrices. The time encoder $h_t(\cdot)$ learns representative features in time-series inputs x_t, and outputs the corresponding feature matrix z_t. In parallel with the time encoder, the frequency encoder $h_f(\cdot)$ outputs feature matrix z_f for the frequency domain inputs x_f. Each encoder is composed by stacking two core modules named *Extraction* and *Concentration blocks*, which are designed to learn effective latent features from the data with periodicity.

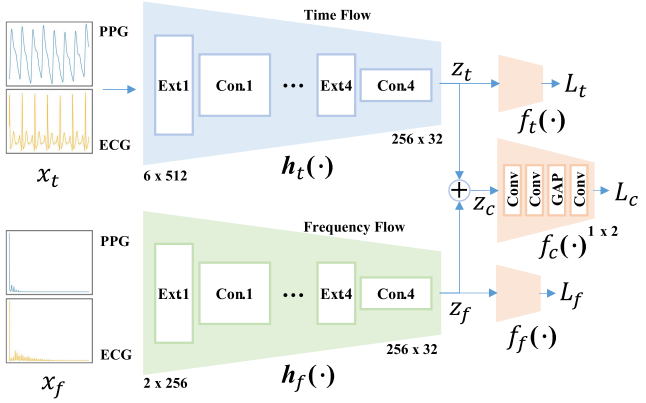

FIGURE 3. Overview of the proposed BP prediction model based on fully convolutional neural networks.

1) EXTRACTION-CONCENTRATION BLOCKS

For CNN to handle periodic sequential data, such as PPG and ECG, the main issue is how the model can learn the relationship between neighboring data points with different intervals unlike images. Two components, multiple dilated convolution and strided convolution with a large kernel, are the main features of our method. We illustrate the detailed structure of *Extraction* and *Concentration blocks* in Fig. 4.

In the *Extraction block* $E(\cdot) : \mathbb{R}^{D \times W} \rightarrow \mathbb{R}^{D \times W}$, where D is the input dimension, and W is the size of input, we use

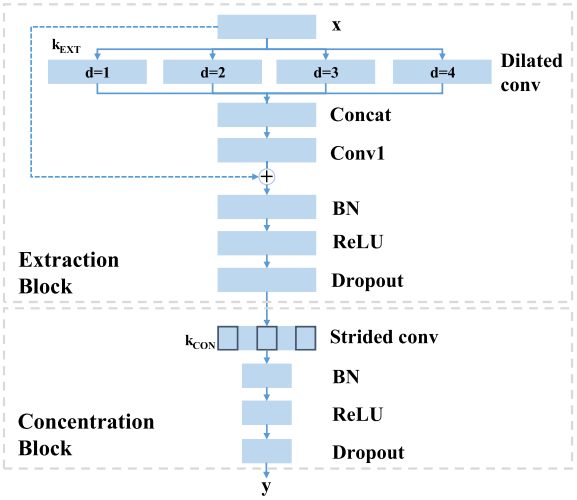

FIGURE 4. Detailed architectures of *Extraction* and *Concentration* blocks.

four parallel dilated convolutions with pre-defined kernel size k_{EXT} and dilation factors of [1, 2, 3, 4]. A model can learn the various relationships between different neighboring pixels within the $4 \times (k_{\text{EXT}} - 1) + 1$ range through multiple dilated convolution. Each output from the multiple dilated convolutions is concatenated together and reduced to the initial dimension by convolution with filter size 1. We use the residual connection, which is a well-known technique to allow better gradient flow. As with temporal convolutional networks (TCN), the combination of batch normalization (BN), ReLU non-linearity, and dropout layer is placed after the residual connection [25].

In the *Concentration block* $C(\cdot) : \mathbb{R}^{D \times W} \rightarrow \mathbb{R}^{D' \times \frac{W}{2}}$, where D is the input dimension, D' is the output dimension, and W is the input size. The model can concentrate the outputs from the *Extraction block* and increase the depth of the features to gain better representations, which lie in a lower dimension space. A typical choice for this concentration is max pooling, but we use a strided convolution with kernel size k_{CON} as an alternative. The reason for this is because there is much information loss by pooling when we apply a large kernel size. We compare the performance between pooling and strided convolution through the experiment in Sec IV. B. After the strided convolution, the BN+ReLU+Dropout combination layer is placed in the same way as the *Extraction block*.

Both the time encoder and the frequency encoder consist of four *Extraction+Concentration* combinations. Another important factor here is the receptive field size. Even though the network is deeply stacked to increase the receptive field, the actual network has a characteristic of focusing on local regions [26]. Therefore, we chose to increase the kernel size instead of deeply configuring the network. Considering the possible heart rate range, an input signal of more than 4 seconds can contain at least 2 periods of the signal, which implies that the input needs to have 500 pixels when using a 125 Hz sampling frequency. The proposed model should therefore have a receptive field size of more than 500 pixels. More precisely, since the inputs to our model have sizes of 512 and 256 for the time and frequency domain respectively, the kernel sizes of each *Extraction* (k_{EXT}) and *Concentration blocks* (k_{CON}) are needed to satisfy these constraints. Possible combinations of the filter sizes for our 4-EC stacked networks are (3, 27, 25), (5, 19, 17) and (7, 11, 9) for (k_{EXT}, k^t_{CON}, k^f_{CON}), where k^t_{CON} and k^f_{CON} are the filter sizes of the *Concentration block* for time and frequency flow. We selected (7, 11, 9) for the experiments, and related results regarding filter sizes will be described in Section IV-B.

2) PREDICTION AND TRAINING

After feature extraction through both time and frequency encoders, we can define the combined feature matrix $z_c = z_t \oplus z_f$. The combined predictor $f_c(\cdot) : \mathbb{R}^{D_c \times W} \rightarrow \mathbb{R}^2$, where D_c is the dimension of z_c and W is the size of z_c, consists of a double stacked convolution layer, global average pooling, and a dimension reduction convolution layer. The output $\hat{y}_c$ of $f_c(\cdot)$ is two real numbers which indicate SBP and DBP. The objective of the prediction is to minimize the distance between the target y and the prediction y_c. L1 and L2 distance are the typical error measurements; we compared the performance of both cases applying the L1 or L2 distance in Sec IV. B. The objective to minimize is defined as:

$$L_c = d(y_c, \hat{y_c}), \tag{5}$$

where d can be any distance metric between real numbers, L1 and L2 in this case.

In addition to this, we added two auxiliary flows from the predictors $f_t(\cdot)$ and $f_f(\cdot)$ which take the pre-concatenated features z_t and z_f as inputs, respectively. Both auxiliary predictors have a simpler structure which consists of one convolution layer, global average pooling, and a dimension reduction convolution layer. Auxiliary loss is a well-known technique to help the model's gradient flow in the back-propagation phase, and will improve performance. We introduce the importance factor α to both losses L_t and L_f. Our final loss is defined as follows:

$$L_{\text{total}} = L_c + \alpha(L_t + L_f) \tag{6}$$

The effect of auxiliary loss will be described in Section IV-B. We can update the model parameters by mini-batch gradient descent with respect to the current model weight. Training details for the experiments will be outlined in Section IV-A.

C. DETAILED ARCHITECTURE

Table 1 shows detailed information about the proposed architecture. It contains the layer structure, input/output dimension, size of kernel/stride/dilation and the receptive fields at each layer.

IV. EXPERIMENTAL RESULTS

A. SETUP

In the experiments, the Cuffless Blood Pressure Estimation dataset is used as a source of the ECG, PPG, and ABP

TABLE 1. Model architecture details.

Arch	Layer	Operation	Size	Out	Kernel	Stride	Dilation	Recep. field
Time	*Ext.1*	Multi-conv	6x512	6	7	1	[1,2,3,4]	25
		BN+ReLU+Dropout						
	Con.1	Conv	6x512	32	11	2	1	35
		BN+ReLU+Dropout						
	Ext.2	Multi-conv	32x256	32	7	1	[1,2,3,4]	83
		BN+ReLU+Dropout						
	Con.2	Conv	32x256	64	11	2	1	103
		BN+ReLU+Dropout						
	Ext.3	Multi-conv	64x128	64	7	1	[1,2,3,4]	199
		BN+ReLU+Dropout						
	Con.3	Conv	64x128	128	11	2	1	239
		BN+ReLU+Dropout						
	Ext.4	Multi-conv	128x64	128	7	1	[1,2,3,4]	431
		BN+ReLU+Dropout						
	Con.4	Conv	128x64	256	11	2	1	511
		BN+ReLU+Dropout						
Freq	*Ext.1*	Multi-conv	2x256	2	7	1	[1,2,3,4]	25
		BN+ReLU+Dropout						
	Con.1	Conv	2x256	32	9	1	1	33
		BN+ReLU+Dropout						
	Ext.2	Multi-conv	32x256	32	7	1	[1,2,3,4]	57
		BN+ReLU+Dropout						
	Con.2	Conv	32x256	64	9	2	1	65
		BN+ReLU+Dropout						
	Ext.3	Multi-conv	64x128	64	7	1	[1,2,3,4]	113
		BN+ReLU+Dropout						
	Con.3	Conv	64x128	128	9	2	1	129
		BN+ReLU+Dropout						
	Ext.4	Multi-conv	128x64	128	7	1	[1,2,3,4]	225
		BN+ReLU+Dropout						
	Con.4	Conv	128x64	256	9	2	1	257
		BN+ReLU+Dropout						
Comb	Layer1	Conv	512x32	512	3	1	1	
		BN+ReLU+Dropout						
	Layer2	Conv	512x32	512	3	1	1	
		BN+ReLU+Dropout						
	Layer3	GAP	512x32	512x1				
		Conv	512x1	2	1	1	1	

signals. This dataset was generated by Kachuee [27], initially collecting ECG, PPG and ABP signals from the Physionet's Multi-parameter Intelligent Monitoring in Intensive Care (MIMIC) II (version 3, accessed on Sept. 2015) online waveform database [28] and then preprocessing to remove the deterioration effects of noise and artifacts from the raw signals. The dataset consists of 12,000 records with all of the ECG, PPG, and ABP signals in hierarchical data format. Each record consists of three rows, with each row corresponding to one signal channel: 125Hz ECG from channel II (ECG lead II), 125Hz PPG from a fingertip, 125Hz invasive ABP. After the data preparation process described in Section III-A., the entire dataset contains 1,912 records from 942 different subjects. We split the dataset into training (70%, 1,340), validation (10%, 193), and test (20%, 379) sets.

For training, we use the Adam optimizer with $\beta_1 = 0.9$, $\beta_2 = 0.999$, a mini-batch size of 100, and no weight decay. The initial learning rate is 0.001 decayed by 0.2 after 800 epochs. The dropout rate is set to 0.2 for the entire networks.

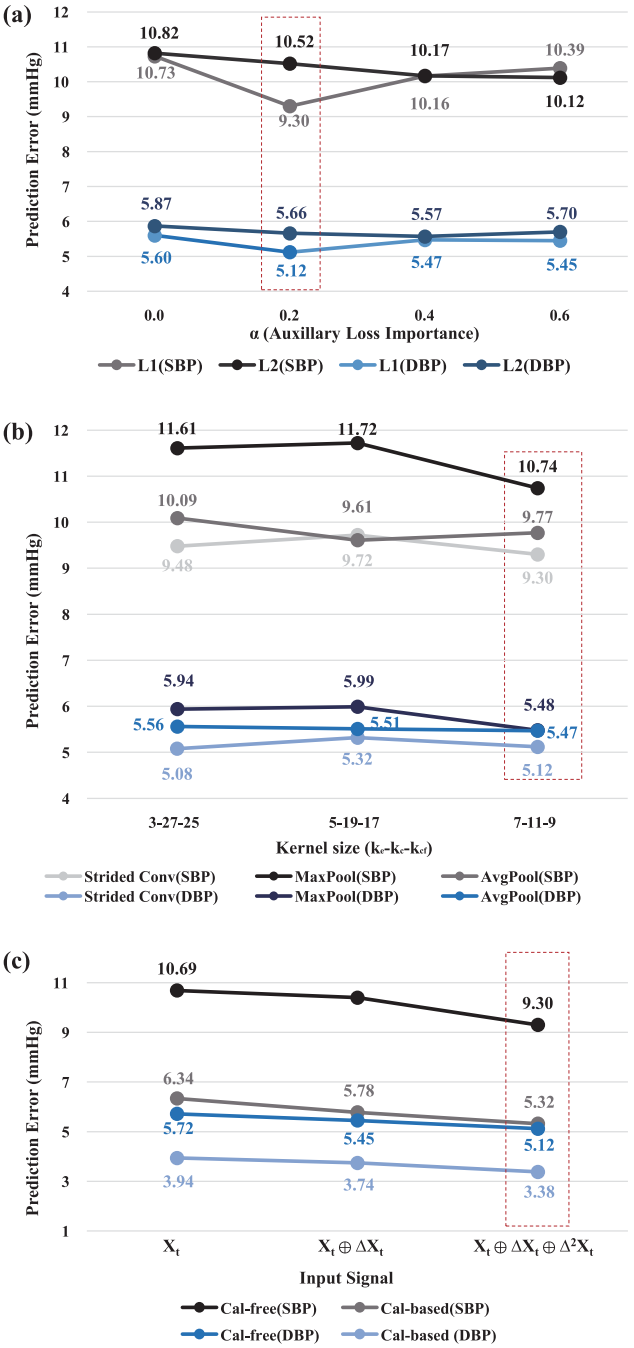

FIGURE 5. BP prediction error analysis according to the model component changes. The best performing model is marked with a red dotted line. (a) BP prediction error due to loss metric and auxiliary weight variation. (b) BP prediction error according to pooling type and kernel size. (c) BP prediction error due to the use of derivatives of the input signals.

B. MODEL EVALUATION AND SELECTION

To investigate the effect of model parameters, we performed prediction error analysis with changes in different components (e.g., loss metric change, the weight of auxiliary loss, type of pooling, kernel size). Fig. 5. shows the difference in prediction error value according to loss metric change (L1, L2), weight of auxiliary loss (0, 0.2, 0.4, 0.6), type

TABLE 2. Comparison of BP prediction accuracy with other related works.

	Dataset	Author	Input	Model	Input	SBP(mmHg)		DBP(mmHg)	
						MAE	STD	MAE	STD
Cal-free	MIMIC II	M. Kachuee [3]	Features	ML ensemble	ECG, PPG	11.17	10.09	5.35	6.14
	MIMIC II	Ours	Raw	CNN	ECG, PPG	**9.30**	8.85	**5.12**	5.52
	Queensland	Y. Zhang [12]	Features	SVM	PPG	11.64	8.20	7.62	6.78
	MIMIC II	Ours	Raw	CNN	PPG	**10.86**	9.54	**5.95**	5.60
Cal-based	MIMIC II	M. Kachuee [3]	Features	ML ensemble	ECG, PPG	8.21	5.45	4.31	3.52
	MIMIC II	Ours	Raw	CNN	ECG, PPG	**5.32**	5.54	**3.38**	3.82
Without train/test data split by subject†	Self-made	P. Su‡ [4]	Features	LSTM	ECG, PPG	3.73‡		2.43‡	
	MIMIC II	O. F. Ertugrul [11]	Features	ELM	ECG, PPG	4.37		3.95	
	Queensland	S. Khalid [9]	Features	Regression tree	PPG	4.82	4.31	3.25	4.17
	MIMIC II	L. Wang [10]	Features	ANN	PPG	4.02	2.79	2.27	1.82
	MIMIC II	O. F. Ertugrul [11]	Features	ELM	PPG	4.25		3.95	

† Training without consideration of train/test data split by subject would result in an abnormally high BP prediction accuracy because the subject data used in the training phase may be used in the test phase.
‡ Root-mean-square-error (RMSE)

of pooling (Strided Conv, MaxPool, AvgPool), and kernel size (filter combination). As can be seen in Fig. 5(a), in the case of using L1 loss, the prediction error is lower than that using L2 loss. In the case of auxiliary loss weight α, a small auxiliary loss weight helps the model's gradient flow in the backpropagation phase, which reduces the prediction error. If a large weight is used, however, the prediction error is increased because L_t and L_f have a greater impact on L_{total} than L_c. The results of the prediction error measurement depending on the pooling type and the kernel size can be seen in Fig. 5(b). In the case of the pooling type, it can be confirmed that the prediction error when using Strided Conv is lower than that when using MaxPool or AvgPool. This is due to the information loss by pooling when we apply a large kernel size. In the case of the combination of filter sizes, we conducted an experiment to compare prediction error for three combinations. It was confirmed that the prediction error of the $k_{\text{EXT}}, k^t_{\text{CON}}, k^f_{\text{CON}} = 7, 11, 9$ combination with the largest k_{EXT} is the lowest because the model can learn the relationship between pixels in a larger neighborhood through a large k_{EXT}. The results of the BP prediction error test with and without input signal's derivative are shown in Fig. 5(c). BP prediction error is lowest when input signal's first and second derivatives are used together with the original signal regardless of the calibration.

Through prediction error analysis with component changes, SBP and DBP prediction performance are the best when using L1 loss, a weight of auxiliary loss $\alpha = 0.2$, Strided Conv, and a combination of $k_{\text{EXT}}, k^t_{\text{CON}}, k^f_{\text{CON}} = 7, 11, 9$. BP prediction performance results are shown in Table 2 with the calibration-based results to be covered in the next section.

C. CALIBRATION-BASED METHOD

The proposed method in this study does not need any calibration to predict BP. However, when using a smart device, such as a telephone or a watch, to repeatedly measure data to estimate the BP, it is possible to improve the accuracy of BP prediction by calibrating the pre-trained models using partial personal data.

To confirm the improvement of the BP prediction accuracy of the calibration based method, test data was divided into several non-overlapping sections. Half of the divided data is used for calibrating the pre-trained model and the remaining data is used to evaluate the BP predictive ability of the calibration-based model. Fig. 6. presents the scatter plots for calibration-free and calibration-based methods, when using the best performance model as selected in the previous section. When comparing the graphs before and after calibration, the scattered points on the graph converge to a straight line through calibration, which can also be confirmed by comparing Pearson's correlation coefficient (r) values before and after calibration in both SBP and DBP. In particular, calibration-based model showed a high Pearson's correlation coefficient of SBP 0.89, DBP 0.80, which

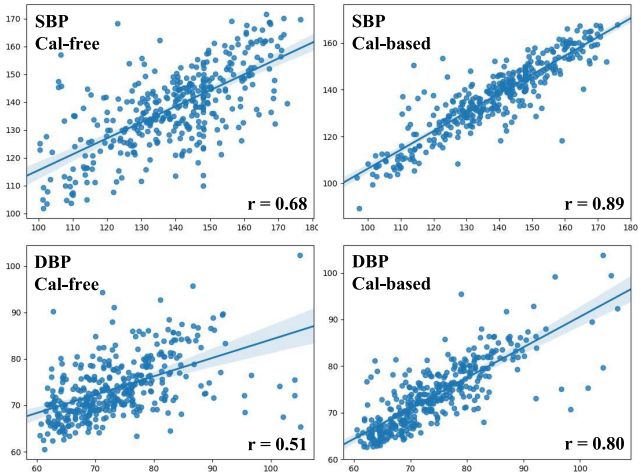

FIGURE 6. Scatter plots for calibration-free and calibration-based models. The x-axis represents the reference value and the y-axis represents the predicted value.

are higher than those shown in other experiments using PWV features (PAT, PTT and so on) and MIMIC dataset [29]. The Pearson's correlation coefficient between blood pressure and PWV features was reported as a value between −0.28 and −0.71. We have confirmed that the features extracted automatically through CNN proposed in this paper are more suitable for predicting blood pressure without cuff than the features extracted manually from other studies.

D. PERFORMANCE COMPARISON

Table 2 shows the comparison of BP prediction accuracy between the proposed method and previous studies. Most studies used mean absolute error (MAE) as an evaluation metric of BP prediction accuracy, and we also compared the results using MAE.

Training without consideration of train/test data split by subject would result in an abnormally high BP prediction accuracy because the subject data used in the training phase may be used in the test phase. For a fair comparison, we did not compare the performance with the results of studies not considering train/test data split by subject [4], [9], [10], [11] and the study using private dataset [4]. We compared only the results obtained under the same conditions in this study.

From the results in Table 2, we can confirm that both the calibration-free and calibration-based BP prediction methods in this study show the best performance compared with other studies. In calibration-free settings, the performances of both ECG+PPG and PPG only improve significantly compared with previous studies: SBP 16.7% (11.17→9.30) and DBP 4.3% (5.35→5.12) with ECG+PPG, SBP 6.7% (11.64→10.86) and DBP 21.9% (7.62→5.95) with PPG only. These results show that the proposed CNN method can work flexibly with various input combinations. An in-depth analysis of this will be described in Section IV-F. Notably, It is encouraging that the improvement with calibration is much more substantial (SBP 35.2%, DBP 21.6%) than the result without calibration. This is due to the strong approximation performance of CNN compared to other machine learning methods. From an application perspective, we can expect that the proposed method will be robust with a wearable device, which requires personalized calibration.

E. VERIFICATION USING INTERNATIONAL STANDARDS FOR BP MEASUREMENT GRADING CRITERIA

1) ASSOCIATION FOR THE ADVANCEMENT OF MEDICAL INSTRUMENTATION (AAMI)

Table 3 presents the verification results of the proposed method using CNN based estimation model with the AAMI standard. The criteria for fulfilling the AAMI protocol are that the test device must not differ from the mercury standard by a mean error (ME) of ≤5 mmHg or a standard deviation (STD) of ≤8 mmHg. According to the AAMI grading criteria, almost all of the calibration-free and calibration-based methods proposed in this study satisfy the AAMI criteria for both BSP and DBP. The standard deviation value of the SBP is slightly over the AAMI standard limit [30].

TABLE 3. Verification with the AAMI standard.

			Diffrence between standard and predicted value(mmHg)		
			ME	STD	Subjects
Proposed	Cal-free	DBP	0.13	7.54	379
		SBP	-1.23	12.80	
	Cal-based	DBP	-0.48	5.08	
		SBP	-1.29	7.58	
AAMI		SBP/DBP	≤ 5	≤ 8	≥85

TABLE 4. Verification with the BHS standard.

			Absolute difference			Grade
			≤ 5	≤ 10	≤ 15	
Proposed	Cal-free	DBP	64.1%	87.1%	95.0%	A
		SBP	40.6%	67.5%	80.2%	D
		MAP	62.0%	87.1%	95.8%	A
	Cal-based	DBP	79.2%	95.3%	97.9%	A
		SBP	59.6%	87.3%	93.7%	B
		MAP	79.7%	96.0%	99.2%	A
BHS		grade A	60%	85%	95%	
		grade B	50%	75%	90%	
		grade C	40%	65%	85%	

2) BRITISH HYPERTENSION SOCIETY (BHS)

Table 4 presents the verification results of the proposed method using CNN based estimation model with the BHS standard. The BHS grading criteria represent the cumulative percentage of readings falling within 5 mmHg, 10 mmHg, and 15 mmHg of the mercury standard. All three percentages must be greater than or equal to the values shown for a specific grade to be awarded. The criteria for fulfilling the BHS protocol are that devices must achieve at least grade B (where A denotes the greatest agreement with mercury standard and D denotes least agreement) for systolic and for diastolic pressures. Mean arterial pressure (MAP) is defined as the average pressure in a patient's arteries during one cardiac cycle. It can be calculated from the SBP and the DBP using the formula [31]:

$$MAP = \frac{SBP + 2(DBP)}{3} \tag{7}$$

According to the BHS grading criteria, the proposed calibration-free method achieved A grade in the prediction of DBP and B grade in the prediction of MAP value. In the case of calibration-free method, for SBP, the proposed method achieved a grade lower than B. After considering the calibration-based method actually in use the proposed method achieved an A grade in DBP and a B grade in SBP predictions. The proposed method satisfies the BHS standard completely except for SBP in the case of calibration-free method [30].

F. PERFORMANCE COMPARISON BY THE INPUT SIGNAL COMBINATIONS

The concept of estimating BP using a single biomedical signal such as PPG or ECG that can be easily measured from a mobile device such as a smartphone or a watch seems to be promising. The same experiment was conducted using a single PPG or ECG signal as the input for the development of the wearable product. Table 5 presents the accuracy of the experiment for different input signal combinations. The accuracy is the best when both the time and frequency encoders of PPG+ECG inputs are used. In the case of using a single ECG or PPG signal, the BP prediction performance is lower than the case of using both input signals together. However, as shown in Table 2, this result shows superior BP prediction performance compared with other previous experiments using the same input signal. In all three cases using ECG+PPG, PPG, and ECG as inputs, it can be seen that the accuracy is higher when time and frequency signals are used together than when only a time or a frequency signal is used. The performance improvement due to the correlation is larger when the time signal is used than the frequency signal. In addition, PPG signal does not seem to be helpful for learning when only frequency domain of PPG signal is used. To verify this result, an ablation experiment was conducted using the input combination where only the frequency encoder of PPG is removed from the best combination (both the time and frequency encoders of PPG+ECG inputs are used). The accuracy of BP prediction was found to be SBP 9.60 $\pm$ 9.53 and DBP 5.14 $\pm$ 5.10 for calibration-free, and SBP 5.98 $\pm$ 6.17 and DBP 3.81 $\pm$ 3.96 for calibration-based, respectively. This result is worse than those of the best combination. This result shows that any relation between time and frequency input contributes to the improvement of BP prediction performance. Our proposed model can learn this relationship to improve accuracy.

TABLE 5. Performance comparison by the input signal combinations: PPG+ECG vs. PPG vs. ECG, Time+Freq. vs. Time vs. Freq.

		Cal-free				Cal-based			
		SBP		DBP		SBP		DBP	
		MAE	STD	MAE	STD	MAE	STD	MAE	STD
Time + Freq.	PPG+ECG	**9.30**	8.85	**5.12**	5.52	**5.32**	5.54	**3.38**	3.82
	PPG only	10.86	9.54	5.95	5.60	7.16	6.79	4.48	4.60
	ECG only	11.46	9.73	5.72	5.55	7.29	6.87	4.39	4.49
Time only	PPG+ECG	10.13	9.48	5.45	5.34	5.93	6.13	3.63	3.83
	PPG only	11.15	9.82	5.71	5.98	7.41	7.02	4.32	4.50
	ECG only	11.57	10.78	5.81	6.00	7.00	6.82	4.14	4.43
Freq. only	PPG+ECG	11.66	10.65	5.95	5.60	9.49	9.14	5.02	5.04
	PPG only	12.43	11.43	6.17	6.14	11.25	10.15	5.85	5.53
	ECG only	11.79	10.30	5.70	5.61	9.33	8.62	4.92	4.55

G. AN ABLATION STUDY OF EACH ARCHITECTURAL COMPONENT OF EXTRACTION-CONCENTRATION BLOCKS

The ablation experiment was conducted using both the time and frequency encoders of PPG+ECG signals together as inputs, to verify the effectiveness of each architectural component on the final accuracy. To verify the effectiveness of each architectural component, we conducted three types of experiment. First, we directly excluded the residual connection inside the *Extraction block* to observe the network performance. Second, we directly excluded the *Extraction block*. Third, we conducted the experiment without the *Concentration block*. However, if the *Concentration block* is removed entirely, down-sampling will not be possible. Hence, we switched the *Concentration block* to the maxpool layer instead of directly excluding the *Concentration block*. Table 6 presents the accuracy of the experiment excluding each architectural component. When the *Extraction block* is removed altogether, the drop-in accuracy is greater than when only the residual connection inside the *Extraction block* is removed. The proposed model can learn the various relationships between different neighboring pixels through the *Extraction block*, which is concatenated with each output of multiple dilated convolutions, simultaneously. Furthermore, the use of strided convolution with a large kernel inside the *Concentration block* has the greatest effect on accuracy improvement. This result shows that considering a wide range of multiple pixels together in the down-sampling step through strided convolution with a large kernel size, instead of pooling in the *Concentration block*, has a significant effect on the improvement of accuracy.

TABLE 6. Performance comparison by excluding architectural components of extraction-concentration blocks.

	Cal-free			
	SBP		DBP	
	MAE	STD	MAE	STD
Final model	**9.30**	8.85	**5.12**	5.52
w/o residual connection	9.87	9.41	5.69	6.61
w/o extraction block	10.47	9.88	6.19	6.86
w/o concentration block	11.51	10.35	6.42	7.22

V. DISCUSSION

In this paper, we designed the filter size to consider wide range which is different from the general filter structure ($k = 3$) used mainly in the field of vision. We believe that the large receptive field due to the wide filter size is more effective in solving the regression problem of the sequential signal than the small receptive field of the general CNN structure. In particular, a multi-dilated convolution based extraction block designed to consider various values (when $k = 7$, 7$\sim$25 pixels around, up to 0.2 seconds) based on a reference pixel has played an important role in improving BP prediction accuracy.

The proposed method can be easily applied to an on-device application for several reasons: 1) It is possible to train and predict BP values using a short time duration (about 8 seconds); 2) It is possible to combine various inputs such as ECG and/or PPG signals to utilize the measurable biomedical

signal according to the conditions of the device; 3) It uses the raw signal as input without unique feature extraction. Notably, an on-device application has the advantage that there is no need for additional equipment or special conditions (synchronization, etc.) for feature extraction.

We applied two constraints to the ABP signal, which is the target value of prediction as a minimum refinement for proper training. No constraints were applied to ECG and PPG used as inputs to training. In other words, we did not exclude any abnormal inputs for training, which allowed us to create a model that is robust to signal measurement errors and noise.

The MIMIC II database used in this paper has several potential limitations on performance improvements: 1) Sampling rate of MIMIC II database is very low for today's minimum recommended 1000 Hz sampling rate [32]. It is expected that the performance improvement will be possible when using data with a higher sampling rate. However, it should be verified whether the proposed model structure and data preprocessing method are still valid. If necessary, it would be possible to propose a new model structure that is effective for high sampling rate data through further studies. 2) It was obtained from intensive care units (ICU), which means that the average age and BP value of subjects are higher than average age and BP value of the total population. We will conduct experiments using large amounts of unbiased data through consultation with medical experts to improve performance.

We propose fully convolutional networks constructed using only 1D convolution for BP prediction. Based on the architecture of CNN, our method has a flexibility to deal with input variations and can predict BP without much consideration of the relationship with previous sequence. Future work will include a detailed inspection of other possible deep architectures for potentially improving the initial results with CNN. From a wearable application perspective, it is essential to calibrate the pre-trained model to fit each individual. In this study, we show that the BP prediction performance of the model is improved through basic calibration using a public dataset. It will become more necessary to study precise calibration technology which is more personalized. Future research will focus on improving personalized BP prediction performance by using private data on the pre-trained model using a public dataset.

VI. CONCLUSION

In this paper, we have developed a calibration-free, cuffless BP prediction method based on the deep CNN model. BP measurement is important in monitoring health conditions to prevent heart disease and stroke. In this method, we can predict BP using ECG and PPG signals that can be easily measured through various sensors without the inconvenience of wearing cuffs. Unlike many previous studies, we have shown that BP can be estimated better than in previous studies by directly using raw signals without any unnecessary preprocessing procedure to extract features from ECG and PPG signals. The performance of this model was verified by comparing with the accuracy of other researchers' previous studies and various international standards for BP measurement grading criteria. Through comparison with international standards, we confirmed that BP prediction accuracy of the method proposed in this paper is sufficiently high to recommend for clinical use.

REFERENCES

[1] R. Merai, "CDC grand rounds: A public health approach to detect and control hypertension," MMWR Morbidity Mortality Weekly Rep. 65, 2016.

[2] S. S. Yoon, C. D. Fryar, and M. D. Carroll, *Hypertension Prevalence and Control Among Adults: United States, 2011–2014*. Hyattsville, MD, USA: US Department of Health and Human Services, Centers for Disease Control and Prevention, National Center for Health Statistics, 2015.

[3] M. Kachuee, M. M. Kiani, H. Mohammadzade, and M. Shabany, "Cuffless blood pressure estimation algorithms for continuous healthcare monitoring," *IEEE Trans. Biomed. Eng.*, vol. 64, no. 4, pp. 859–869, Apr. 2017.

[4] P. Su, X.-R. Ding, Y.-T. Zhang, J. Liu, F. Miao, and N. Zhao, "Long-term blood pressure prediction with deep recurrent neural networks," in *Proc. IEEE EMBS Int. Conf. Biomed. Health Inform. (BHI)*, Mar. 2018, pp. 323–328.

[5] R. Mukkamala, J.-O. Hahn, O. T. Inan, L. K. Mestha, C.-S. Kim, H. Töreyin, and S. Kyal, "Toward ubiquitous blood pressure monitoring via pulse transit time: Theory and practice," *IEEE Trans. Biomed. Eng.*, vol. 62, no. 8, pp. 1879–1901, Jun. 2015.

[6] X. Ding, B. P. Yan, Y.-T. Zhang, J. Liu, N. Zhao, and H. K. Tsang, "Pulse transit time based continuous cuffless blood pressure estimation: A new extension and a comprehensive evaluation," *Sci. Rep.*, vol. 7, no. 1, 2017, Art. no. 11554.

[7] H. Gesche, D. Grosskurth, G. Küchler, and A. Patzak, "Continuous blood pressure measurement by using the pulse transit time: Comparison to a cuff-based method," *Eur. J. Appl. Physiol.*, vol. 112, no. 1, pp. 309–315, 2012.

[8] W. Chen, T. Kobayashi, S. Ichikawa, Y. Takeuchi, and T. Togawa, "Continuous estimation of systolic blood pressure using the pulse arrival time and intermittent calibration," *Med. Biol. Eng. Comput.*, vol. 38, no. 5, pp. 569–574, 2000.

[9] S. G. Khalid, J. Zhang, F. Chen, and D. Zheng, "Blood pressure estimation using photoplethysmography only: Comparison between different machine learning approaches," *J. Healthcare Eng.*, vol. 2018, Oct. 2018, Art. no. 1548647.

[10] L. Wang, W. Zhou, Y. Xing, and X. Zhou, "A novel neural network model for blood pressure estimation using photoplethesmography without electrocardiogram," *J. Healthcare Eng.*, vol. 2018, Mar. 2018, Art. no. 7804243.

[11] Ö. F. Ertuğrul and N. Sezgin, "A noninvasive time-frequency-based approach to estimate cuffless arterial blood pressure," *Turkish J. Elect. Eng. Comput. Sci.*, vol. 26, no. 5, pp. 2260–2274, 2018.

[12] Y. Zhang and Z. Feng, "A SVM method for continuous blood pressure estimation from a PPG signal," in *Proc. ACM 9th Int. Conf. Mach. Learn. Comput.*, 2017, pp. 128–132.

[13] M. Sharma, K. Barbosa, V. Ho, D. Griggs, T. Ghirmai, S. Krishnan, T. Hsiai, J.-C. Chiao, and H. Cao, "Cuff-less and continuous blood pressure monitoring: A methodological review," *Technologies*, vol. 5, no. 2, p. 21, 2017.

[14] C. Vlachopoulos, M. O'Rourke, and W. W. Nichols, *McDonald's Blood Flow in Arteries: Theoretical, Experimental and Clinical Principles*. Boca Raton, FL, USA: CRC Press, 2011.

[15] M. S. Tanveer and M. K. Hasan, "Cuffless blood pressure estimation from electrocardiogram and photoplethysmogram using waveform based ANN-LSTM network," *Biomed. Signal Process. Control*, vol. 51, pp. 382–392, May 2019.

[16] Y. Liang, Z. Chen, R. Ward, and M. Elgendi, "Photoplethysmography and deep learning: Enhancing hypertension risk stratification," *Biosensors*, vol. 8, no. 4, p. 101, 2018.

[17] Y. LeCun, Y. Bengio, and G. Hinton, "Deep learning," *Nature*, vol. 521, no. 7553, p. 436, 2015.

[18] I. Sutskever, G. E. Hinton, and A. Krizhevsky, "Imagenet classification with deep convolutional neural networks," in *Proc. Adv. Neural Inf. Process. Syst.*, 2012, pp. 1097–1105.
[19] Q. Zhang, L. T. Yang, Z. Chen, and P. Li, "A survey on deep learning for big data," *Inf. Fusion*, vol. 42, pp. 146–157, Jul. 2018.
[20] K. Sirinukunwattana, S. E. A. Raza, Y.-W. Tsang, D. R. J. Snead, I. A. Cree, and N. M. Rajpoot, "Locality sensitive deep learning for detection and classification of nuclei in routine colon cancer histology images," *IEEE Trans. Med. Imag.*, vol. 35, no. 5, pp. 1196–1206, May 2016.
[21] H.-S. Choi, J. Y. Choe, H. Kim, J. W. Han, Y. K. Chi, K. Kim, J. Hong, T. Kim, T. H. Kim, and S. Yoon, "Deep learning based low-cost high-accuracy diagnostic framework for dementia using comprehensive neuropsychological assessment profiles," *BMC Geriatrics*, vol. 18, no. 1, p. 234, 2018.
[22] V. Dumoulin and F. Visin, "A guide to convolution arithmetic for deep learning," 2016, *arXiv:1603.07285*. [Online]. Available: https://arxiv.org/abs/1603.07285
[23] A. V. Chobanian, G. L. Bakris, H. R. Black, W. C. Cushman, L. A. Green, J. L. Izzo, Jr., D. W. Jones, B. J. Materson, S. Oparil, and J. T. Wright, Jr., "The seventh report of the joint national committee on prevention, detection, evaluation, and treatment of high blood pressure: The JNC 7 report," *Jama*, vol. 289, no. 19, pp. 2560–2571, 2003.
[24] Y. Liang, Z. Chen, R. Ward, and M. Elgendi, "Hypertension assessment via ECG and PPG signals: An evaluation using MIMIC database," *Diagnostics*, vol. 8, no. 3, p. 65, 2018.
[25] S. Bai, J. Z. Kolter, and V. Koltun, "An empirical evaluation of generic convolutional and recurrent networks for sequence modeling," 2018, *arXiv:1803.01271*. [Online]. Available: https://arxiv.org/abs/1803.01271
[26] W. Luo, Y. Li, R. Urtasun, and R. Zemel, "Understanding the effective receptive field in deep convolutional neural networks," in *Proc. Adv. Neural Inf. Process. Syst.*, 2016, pp. 4898–4906.
[27] M. Kachuee, M. M. Kiani, H. Mohammadzade, and M. Shabany, "Cuff-less high-accuracy calibration-free blood pressure estimation using pulse transit time," in *Proc. IEEE Int. Symp. Circuits Syst. (ISCAS)*, May 2015, pp. 1006–1009.
[28] M. Saeed, M. Villarroel, A. T. Reisner, G. Clifford, L.-W. Lehman, G. Moody, T. Heldt, T. H. Kyaw, B. Moody, and R. G. Mark, "Multiparameter intelligent monitoring in intensive care II (MIMIC-II): A public-access intensive care unit database," *Critical Care Med.*, vol. 39, no. 5, p. 952, 2011.
[29] Y. Liang, D. Abbott, N. Howard, K. Lim, R. Ward, and M. Elgendi, "How effective is pulse arrival time for evaluating blood pressure? Challenges and recommendations from a study using the mimic database," *J. Clin. Med.*, vol. 8, no. 3, p. 337, 2019.
[30] E. O'Brien, B. Waeber, G. Parati, J. Staessen, and M. G. Myers, "Blood pressure measuring devices: Recommendations of the European society of hypertension," *BMJ*, vol. 322, no. 7285, pp. 531–536, 2001.
[31] R. P. Dellinger, M. M. Levy, A. Rhodes, D. Annane, H. Gerlach, S. M. Opal, J. E. Sevransky, C. L. Sprung, I. S. Douglas, and R. Jaeschke, "Surviving sepsis campaign: International guidelines for management of severe sepsis and septic shock, 2012," *Intensive Care Med.*, vol. 39, no. 2, pp. 165–228, 2013.
[32] O. Kwon, J. Jeong, H. B. Kim, I. H. Kwon, S. Y. Park, J. E. Kim, and Y. Choi, "Electrocardiogram sampling frequency range acceptable for heart rate variability analysis," *Healthcare Inform. Res.*, vol. 24, no. 3, pp. 198–206, 2018.

SANGHYUN BAEK is currently pursuing the Ph.D. degree with the Department of Electrical and Computer Engineering, Seoul National University, Seoul, South Korea. He is currently working as a Researcher with Samsung Electronics. His research interests include deep learning and biomedical signal processing.

JIYONG JANG is currently pursuing the M.S. degree with the Department of Electrical and Computer Engineering, Seoul National University, Seoul, South Korea. He is currently working as a Researcher with Samsung Electronics. His research interests include deep learning and its applications.

SUNGROH YOON (S'99–M'06–SM'11) received the B.S. degree in electrical engineering from Seoul National University, South Korea, in 1996, and the M.S. and Ph.D. degrees in electrical engineering from Stanford University, CA, USA, in 2002 and 2006, respectively. From 2006 to 2007, he was with Intel Corporation, Santa Clara, CA, USA. He was an Assistant Professor with the School of Electrical Engineering, Korea University, from 2007 to 2012. From 2016 to 2017, he was a Visiting Faculty with the Department of Neurology and Neurological Sciences, Stanford University. He held Research positions with Stanford University and Synopsys, Inc., Mountain View, CA, USA. He is currently a Professor with the Department of Electrical and Computer Engineering, Seoul National University. His research interests include artificial intelligence, machine learning, deep learning, and large-scale applications of artificial intelligence and machine learning. He was the recipient of the 2013 IEEE/IEEK Joint Award for Young IT Engineers.